Acta Biomaterialia 168 (2023) 113–124

Contents lists available at ScienceDirect

Acta Biomaterialia

journal homepage: www.elsevier.com/locate/actbio

Full length article

Human nasal cartilage: Functional properties and structure-function relationships for the development of tissue engineering design criteria

Wendy E. Brown, Laura Lavernia, Benjamin J. Bielajew, Jerry C. Hu, Kyriacos A. Athanasiou*

Department of Biomedical Engineering, University of California Irvine, 3120 Natural Sciences II, Irvine, CA, 92697, USA

ARTICLE INFO

Article history:
Received 25 March 2023
Revised 6 July 2023
Accepted 11 July 2023
Available online 16 July 2023

Keywords:
Nose cartilage
Mechanical properties
Biochemical content
Septum
Upper lateral and lower lateral
Alar

ABSTRACT

Nose reconstruction often requires scarce cartilage grafts. Nasal cartilage properties must be determined to serve as design criteria for engineering grafts. Thus, mechanical and biochemical properties were obtained in multiple locations of human nasal septum, upper lateral cartilage (ULC), and lower lateral cartilage (LLC). Within each region, no statistical differences among locations were detected, but anisotropy at some septum locations was noted. In the LLC, the tensile modulus and ultimate tensile strength (UTS) in the inferior-superior direction were statistically greater than in the anterior-posterior direction. Cartilage from all regions exhibited hyperelasticity in tension, but regions varied in degree of hyalinicity (i.e., Col II:Col I ratio). The septum contained the most collagen II and least collagen I and III, making it more hyaline than the ULC and LLC. The septum had a greater aggregate modulus, UTS, and lower total collagen/wet weight (Col/WW) than the ULC and LLC. The ULC had greater tensile modulus, DNA/WW, and lower glycosaminoglycan/WW than the septum and LLC. The ULC had a greater pyridinoline/Col than the septum. Histological staining suggested the presence of chondrons in all regions. In the ULC and LLC, tensile modulus correlated with total collagen content, while aggregate modulus correlated with pyridinoline content and weakly with pentosidine content. However, future studies should be performed to validate these proposed structure-function relationships. This study of human nasal cartilage provides 1) crucial design criteria for nasal cartilage tissue engineering efforts, 2) quantification of major and minor collagen subtypes and crosslinks, and 3) structure-function relationships. Surprisingly, the large mechanical properties found, particularly in the septum, suggests that nasal cartilage may experience higher-than-expected mechanical loads.

Statement of significance

While tissue engineering holds promise to generate much-needed cartilage grafts for nasal reconstruction, little is known about nasal cartilage from an engineering perspective. In this study, the mechanical and biochemical properties of the septum, upper lateral cartilage (ULC), and lower lateral cartilage (LLC) were evaluated using cartilage-specific methods. For the first time in this tissue, all major and minor collagens and collagen crosslinks were measured, demonstrating that the septum was more hyaline than the ULC and LLC. Additionally, new structure-function relationships in the ULC and LLC were identified. This study greatly expands upon the quantitative understanding of human nasal cartilage and provides crucial engineering design criteria for much-needed nasal cartilage tissue engineering efforts.

1. Introduction

Surgeries that require the use of cartilage grafts for repair or reconstruction of nasal cartilage structures are common. For example, the nose is the most common site for facial skin cancer (~36%), and the related tumor resection often damages nasal cartilage [1,2]. Up to 70% of patients at civilian burn centers have burns involving the nose, leading to infection, scarring, and wound contracture that create significant nasal deformities and airway restriction [3]. Injuries to nasal cartilage are particularly prevalent for military personnel due to blast or burn injuries. For example, 44% of evacuations from combat zones between 2001-2011 were

* Corresponding author.
E-mail address: athens@uci.edu (K.A. Athanasiou).

https://doi.org/10.1016/j.actbio.2023.07.011

due to mid-face trauma affecting the nose [4]. Failure to restore nasal function has devastating physical and psychological health ramifications. For example, airway obstruction is known to cause chronic sinus infections, nosebleeds, headaches, insomnia, sleep apnea, and impairment to cognitive function [5–7]. Nasal deformities negatively affect personal development and self-esteem, as well as perception of employability, honesty, and trustworthiness [8]. Rhinoplasty and septoplasty procedures are crucial to reconstructing nasal cartilage following pathology or trauma to prevent negative health impacts.

Reconstructive rhinoplasty and septoplasty require large, mechanically robust grafts. To achieve structural support of the upper third of the nose, rigid reconstruction requires septal or rib (costal) cartilage grafts [9]. Auricular cartilage is frequently used to reconstruct the lower lateral cartilage. Auricular cartilage is also used, along with septal cartilage, for structural grafts in the tip [9,10]. Septal cartilage is generally highly desirable for use as structural graft material because it is strong and straight. However, the limited amount of septal cartilage that may be removed without compromising the structural integrity of the nose often creates a shortage of graft material, especially in cases involving resection or trauma of the septum [9]. The use of ear and costal cartilages may be limited by form factor (i.e., size and shape), availability, and considerable post-implantation warping [11]. Irradiated costal cartilage allografts are used when sufficient amounts of autologous graft tissue are not available. However, these grafts are associated with higher resorption rates than autografts [12,13]. Synthetic or alloplastic nasal implants are commercially available as an alternative to tissue grafts, but are not frequently employed in the US because their use is plagued by inflammation, infection, resorption, dislocation, and extrusion [14–17]. While over $1.1 billion was spent on rhinoplasty in the US in 2016 [18], the surgical revision rate was high (15.5%) [19,20], with 13% of patients retaining the anatomic nasal deformity after surgery [19]. These outcomes emphasize current limitations of graft use in rhinoplasty and motivate the development of tissue-engineered cartilage replacements for nasal reconstruction.

While tissue engineering holds promise to address the need for nasal cartilage grafts, little is known about nasal cartilage from an engineering perspective. Although it has been established that human nasal cartilage is hyaline, previous studies have yielded inconsistent measurements of collagen content, glycosaminoglycan (GAG) content, cellularity, and GAG-to-collagen ratios [21–23]. In terms of mechanics, the L-strut portion of the septum (Fig. 1), or the L-shaped region remaining after septum resection during septoplasty or graft harvesting, has been the most extensively characterized. Several studies have been performed to elucidate the minimum width and thickness of the L-strut to avoid nasal collapse [24,25]. However, the material properties of human nasal cartilage have been primarily characterized using a homogeneous, elastic model in compression and testing methods that are not standardized [26–29]. Furthermore, the septum has primarily been the focus of characterization, with few studies quantitatively examining the upper lateral cartilage (ULC) and lower lateral cartilage (LLC), also known as alar cartilage [27,29-31]. Full characterization of the biochemical content and material properties of all regions nasal cartilage is required to establish engineering design criteria for biomimetic tissue engineering.

Toward generating engineering design criteria for cartilage tissue engineering efforts, the objectives of this study were to 1) provide a comprehensive and quantitative characterization of human nasal cartilage and 2) identify structure-function relationships in human nasal cartilage. It was hypothesized that functional properties would vary by region (septum, ULC, and LLC) of the nose, but not by location within region. To determine locational differences, quantitative properties were first compared among testing locations within each cartilage region. Second, anisotropy was examined by comparing tensile properties in perpendicular directions (inferior-superior (IS) versus anterior-posterior (AP)) at all locations within each cartilage region and in each region, overall. Third, to determine regional differences, quantitative properties from the locations within each region were pooled, and the overall functional properties were compared among the regions of the nose. Structure-function relationships were elucidated by correlating mechanical properties and biochemical contents matched by location.

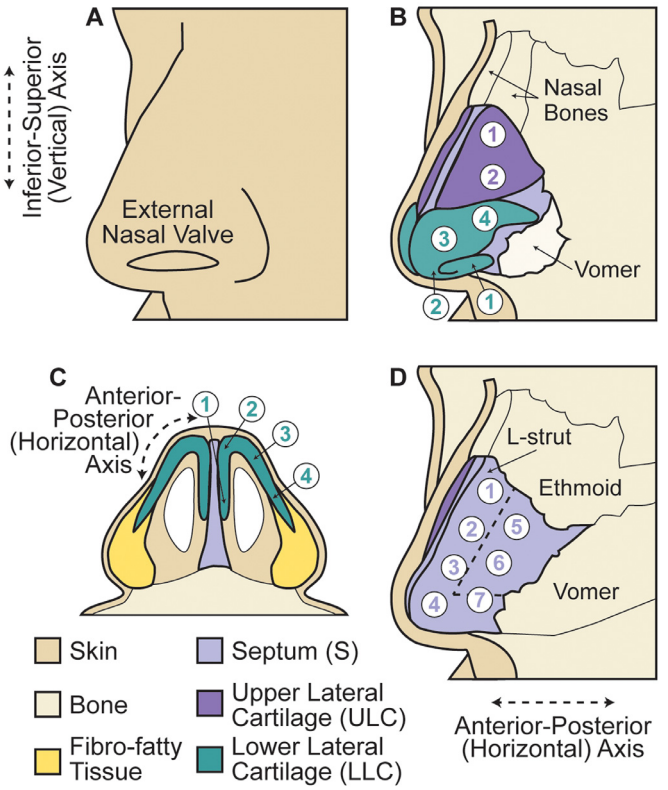

Fig. 1. Anatomy, testing locations, and regions: A) The external nasal valve showing the inferior-superior (IS) testing direction; B) the nose with the skin resected showing juxtaposition of the upper lateral cartilage (ULC) and lower lateral cartilage (LLC) and testing locations on the ULC and LLC; C) testing locations on the LLC, as well as illustration of the anterior-posterior (AP) testing direction; D) illustration of the septum (S) with the ULC and LLC resected showing testing locations, the L-strut, and the AP testing direction.

2. Materials and methods

2.1. Native tissue isolation and sample preparation

Human noses, resected *en bloc* from surrounding tissues, were obtained from the Willed Body program at the University of California Irvine; tissues were Institutional Review Board (IRB)-exempt. Noses were obtained from 8 (four female and four male) Caucasian donors aged between 60-100 years old. Samples were frozen at -80°C for <6 months until processing. In preparation for processing, samples were thawed overnight at 4°C and then allowed to reach room temperature before processing and testing. The cartilage was removed from the surrounding bone and connective tissue and divided into the three anatomical regions (septum (S), ULC, and LLC), taking care to preserve the anatomical orientation with respect to the nasal, ethmoid, and vomer bones (Fig. 1). All nasal cartilage was grossly examined for signs of trauma (e.g., septal breakage) or previous surgery (e.g., septoplasty or rhinoplasty), which represent

exclusion criteria for this study. None of the nasal cartilage displayed signs of these conditions. Therefore, noses from all 8 donors were included in the study.

Subsequently, each region was further subdivided into locations; i.e., the septum was divided into seven locations (S1-7; Fig. 1D), the ULC was divided into two locations (ULC1 and ULC2; Fig. 1B), and the LLC was divided into four locations (LLC1-4; Fig. 1B,C). Samples for all tests were removed from the middle portion of each location and were immediately mechanically tested, saved for biochemical analyses, or preserved for histology.

Samples for compression testing were isolated by punching a 3 mm-diameter disc from each location. Rectangular samples were taken in both the IS (vertical) axis and AP direction (horizontal) axis from each location for tension testing. The residual tissue from each location that was not used for mechanical testing was apportioned for biochemical assays and histology. After dissection and prior to testing or storage for further analysis, sample hydration was maintained by submerging samples in protease inhibitor containing NaCl 8.766g, EDTA 0.673g, benzamidine HCl 0.783g, N-ethylmaleimide 1.251g, and phenylmethylsulfonylfluoride 0.174g per liter of water.

2.2. Mechanical characterization

Creep indentation testing was performed by applying a 1 mm-diameter, flat, porous indenter tip to the center of the cylindrical cartilage punches under loads ranging from 0.01-0.07 N in a bath of phosphate buffered saline. Creep compression was determined by continuously measuring the indenter position [32,33]. Values for the aggregate modulus, shear modulus, and permeability were obtained from the experimental data using a semi-analytical, semi-numerical, linear biphasic model and finite element analysis [32].

Uniaxial tensile testing was also performed. The rectangular samples isolated for tension testing were trimmed to form dog bone-shaped specimens with a gauge length of 1.3 mm. Paper tabs were glued to the specimens outside the gauge length and gripped in a TestResources uniaxial tester (TestResources Inc.). The tabs were pulled parallel to the long axis of the specimen at a rate of 1% of the gauge length per second until sample failure. Stress-strain curves were generated using the cross-sectional area of samples measured with ImageJ. A least-squares fit of the linear region of the curve yielded the tensile modulus, and the maximum stress achieved yielded the ultimate tensile strength (UTS).

2.3. Biochemical characterization

Samples at each location were saved for biochemical analyses, including colorimetric assays, mass spectrometry, and bottom-up proteomic analysis. A sample size of 5 per testing location was used and samples were collected via randomized assignment from the 8 processed noses. No two samples from the same location for the same assay were collected from the same nose. All samples were weighed to obtain wet weights (WW), frozen and lyophilized, and weighed again to obtain dry weights (DW). Samples for colorimetric assays were digested in 125 μg/mL papain in phosphate buffer at 60°C for 18 hours. A Blyscan dimethyl methylene blue assay kit (Biocolor, Ltd) was used to measure sulfated GAG content per manufacturer's instructions. A modified colorimetric chloramine-T hydroxyproline assay using hydrochloric acid [34] and a Sircol collagen assay standard (Biocolor, Ltd) was used to quantify total collagen content (Col). DNA content was measured by performing a Picogreen assay (Quant-iT Picogreen dsDNA assay kit) per manufacturer's instructions. All samples were assayed for GAG and collagen in triplicate, and triplicate values were averaged to yield one representative value per sample. GAG and collagen contents were normalized to WW, DW, and DNA.

Quantification of collagen crosslinks was performed as previously described [35]. Briefly, samples were hydrolyzed in HCl, and hydrolysates were subjected to aqueous normal phase chromatography and mass spectrometry with a quadrupole mass spectrometer (Waters ACQUITY QDa) to quantify pyridinoline (Pyr) and pentosidine (Pent) crosslinks. Both types of crosslinks were normalized to WW, DW, and Col from the hydroxyproline assay.

Bottom-up proteomics was performed, as previously described [35], to measure the content of all major and minor collagen types by region. Briefly, samples were digested in trypsin and combined in equal proportions to yield one "combination sample" per region per nose. Samples were subjected to reverse-phase chromatography and tandem mass spectrometry on an Orbitrap Fusion Lumos mass spectrometer (Thermo Fisher Scientific). Subsequently, label-free quantification was performed with MaxQuant to quantify all identified proteins, normalized to total protein content (Prot). Dividing Col/DW and Col/WW from the hydroxyproline assay by the sum of collagen proteins per total protein (Col/Prot) from bottom-up proteomics yielded Prot/DW and Prot/WW. These values were multiplied by the bottom-up proteomics result for each collagen subtype (e.g., Col II/Prot) to yield normalizations by weight (e.g., Col II/WW and Col II/DW). Collagen subtypes were also compared to the sum of all measured collagen subtypes to yield individual collagen ratios (e.g., Col II/Col).

2.4. Histological evaluation

After fixation in 10% neutral buffered formalin, samples were dehydrated, embedded in paraffin, and sectioned to a thickness of 4 μm to expose the full thickness cross section (i.e., the entire depth of the cartilage) of the tissue. Sections were stained with hematoxylin & eosin (H&E) to illustrate tissue and cell morphology, safranin-O/fast green to visualize GAGs, and picrosirius red to visualize collagen. Picrosirius red-stained slides were also imaged under polarized light microscopy to observe collagen alignment [36].

2.5. Statistical analysis

First, all quantitative data were tested for normality using a Shapiro-Wilk test. In the first level of analysis, the quantitative functional properties (i.e., mechanical properties and biochemical composition) of the nasal cartilage at the locations within each anatomical region (e.g., the septum) were compared. A one-way analysis of variance test (ANOVA), followed by a Tukey's *post hoc* test, was performed to compare the seven locations within the septum. A Student's t-test was performed comparing the two locations within the ULC. A one-way ANOVA and Tukey's *post hoc* test was used to compare the four locations within the LLC.

In the second level of analysis, anisotropy of tensile properties was compared at each location and in each region overall. At each location, tensile results were compared in the IS and AP directions using a Student's t-test. Anisotropy index, which yields a value indicative of the degree of anisotropy, was also calculated by dividing the tensile property in the IS direction by the AP direction. To examine regional anisotropy, tensile results in the IS direction were pooled within each region and compared with the pooled tensile results in the AP direction using a Student's t-test.

In the third level of analysis, the functional properties of the anatomical regions of the nose were compared. One-way ANOVAs with Tukey's *post hoc* tests were performed on the data pooled from each region to compare data across the septum, ULC, and LLC. For the purpose of this study, the 'structure' of matrix components refers to measurable physical properties, such as the quantity of glycosaminoglycans, collagen, and collagen crosslinks. The function of cartilage refers to the measurable material characteristics of the

Table 1
Mechanical properties of the septum, ULC, and LLC by location: For each mechanical property, one-way ANOVAs were performed among locations in the S and among locations in the LLC regions. Likewise, a Student's t-test was performed among locations in the ULC. No statistical differences in mechanical properties were observed among locations within each region.

Location		Aggregate Modulus (kPa)	Shear Modulus (kPa)	Permeability E-15 (m^4/N·s)	Tensile Modulus (MPa)	Ultimate Tensile Strength (MPa)
S	**1**	432 ± 271	204 ± 139	12.3 ± 12.7	5.1 ± 2.1	3.2 ± 1.4
	2	346 ± 166	168 ± 73	12.4 ± 11.7	9.7 ± 3.6	3.9 ± 3.0
	3	367 ± 83	206 ± 55	13.0 ± 8.3	9.2 ± 2.0	4.0 ± 1.7
	4	283 ± 105	157 ± 57	12.6 ± 11.9	7.8 ± 0.5	3.7 ± 1.2
	5	403 ± 219	176 ± 62	14.2 ± 7.7	5.8 ± 3.5	1.7 ± 1.0
	6	449 ± 231	216 ± 128	25.4 ± 18.4	4.6 ± 2.0	1.6 ± 1.0
	7	429 ± 228	279 ± 160	14.1 ± 10.0	10.1 ± 3.1	3.5 ± 2.5
ULC	**1**	171 ± 83	61 ± 28	29.4 ± 10.3	7.1 ± 6.0	2.8 ± 1.1
	2	199 ± 145	119 ± 141	40.2 ± 19.9	13.6 ± 3.4	5.3 ± 2.3
LLC	**1**	239 ± 101	118 ± 49	27.1 ± 28.7	4.1 ± 2.8	2.0 ± 1.4
	2	156 ± 81	121 ± 111	31.3 ± 36.6	4.2 ± 2.2	2.5 ± 1.1
	3	155 ± 69	78 ± 34	56.0 ± 29.3	6.0 ± 3.1	4.2 ± 1.4
	4	186 ± 74	89 ± 22	16.4 ± 13.8	6.8 ± 3.5	3.2 ± 1.9

overall tissue, such as the tensile stiffness and viscoelastic measures (such as the aggregate modulus) [37]. Structure-function relationships were elucidated by calculating location-matched Pearson correlation coefficients between mechanical properties and contents of extracellular matrix molecules known to influence cartilage structure [38,39].

All statistical analyses were performed in Prism 9 software (GraphPad). Significance for all statistical analyses was determined by $p < 0.05$. Quantitative data in figures and tables are presented as means ± standard deviations. A connecting letters report is used to show statistical significance in all bar graphs and tables; bars in graphs or cells in tables that show different letters are significantly different from each other [40].

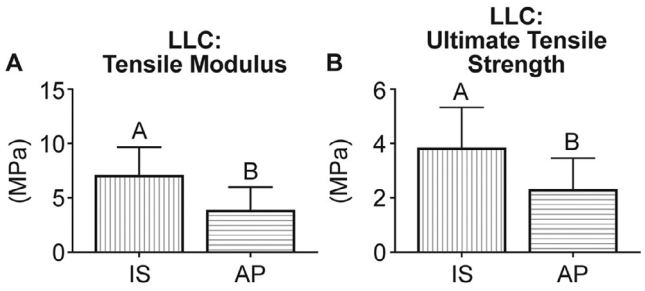

Fig. 2. Anisotropic tensile properties of the LLC: A Student's t-test was performed to compare tensile data between the IS and AP directions, pooled by testing direction. Analysis revealed overall anisotropy in the LLC, where the A) tensile modulus and B) UTS were greater in the IS direction.

3. Results

3.1. Examination of functional properties within each region of the nose

In the first level of analysis, the functional properties at multiple locations within each anatomical region (i.e., septum, ULC, and LLC) were compared. Comparing the seven locations within the septum to each other revealed no statistical differences in aggregate modulus, shear modulus, permeability, tensile modulus, or UTS (Table 1). Similarly, among the septum locations, there were no differences in DNA content normalized to WW and DW or hydration. There were no differences in GAG content and Col content normalized to WW, DW, and DNA. Additionally, there were no differences in Pyr and Pent content normalized to WW, DW, and Col. Hydration, DNA/WW, GAG/WW, Col/WW, Pyr/Col, and Pent/Col by location in the septum are shown in Table 2, with the remaining biochemical data presented in Supplemental Table 1.

When comparing between the two locations in the ULC, there were no statistical differences in aggregate modulus, shear modulus, permeability, tensile modulus, or UTS (Table 1). Similarly, there were no differences in DNA content normalized to WW and DW or hydration. There were no differences in GAG content and Col content normalized to WW, DW, and DNA. Additionally, there were no differences in Pyr and Pent content normalized to WW, DW, and Col. Hydration, DNA/WW, GAG/WW, Col/WW, Pyr/Col, and Pent/Col by location in the ULC are shown in Table 2, with the remaining biochemical data in Supplemental Table 1.

When comparing among the four locations in the LLC, there were no statistical differences in aggregate modulus, shear modulus, permeability, tensile modulus, or UTS (Table 1). Similarly, there were no differences in DNA content normalized to WW and DW or hydration. There were no differences in GAG and Col content normalized to WW, DW, and DNA. There were also no differences in Pyr and Pent content normalized to WW, DW, and Col. Hydration, DNA/WW, GAG/WW, Col/WW, Pyr/Col, and Pent/Col by location in the LLC are shown in Table 2, with the remaining biochemical data shown in Supplemental Table 1.

3.2. Examination of tensile anisotropy within each region of the nose

In the second level of analysis, anisotropy at each location and regions of the nose was examined. Anisotropy of the tensile modulus was observed at locations S1, S2, and S3, as well as LLC4 (Table 3). The tensile modulus was greater in the AP direction at S1. However, at S2 and S3, the tensile modulus was greater in the IS direction. At LLC4, the tensile modulus was greatest in the IS direction. Anisotropy index was calculated for all locations (Table 3). The closer the anisotropy index is to 1, the less anisotropy exists. To examine regional anisotropy, tensile data from all locations within each region were pooled by testing direction (IS or AP). By comparing the data generated by testing in the IS and AP directions, overall anisotropy was revealed in the LLC. The LLC had a greater tensile modulus and UTS in the IS direction than the AP direction (Fig. 2). There were no statistical differences between the IS and AP directions in the tensile moduli or UTS of the septum of ULC.

Collagen alignment was examined via polarized light microscopy. Excluding the perichondrium, collagen alignment was detected to a minor degree in the ULC and LLC, but not the septum.

Table 2
Biochemical content of the septum, ULC, and LLC by location: For each biochemical content, one-way ANOVAs were performed among locations in the S and among locations in the LLC regions. Likewise, a Student's t-test was performed among locations in the ULC. No statistical differences in biochemical contents were observed among locations within each region.

Location		Hydration (%)	DNA/WW (ng/μg)	GAG/WW (%)	Col/WW (%)	Pyr/Col (ng/mg)	Pent/Col (ng/mg)
S	**1**	77.2 ± 1.8	0.16 ± 0.04	3.4 ± 1.1	9.3 ± 4.5	206.7 ± 61.3	19.2 ± 7.2
	2	76.2 ± 1.7	0.18 ± 0.03	3.5 ± 1.4	13.2 ± 1.4	218.0 ± 42.9	20.4 ± 6.4
	3	74.3 ± 2.1	0.18 ± 0.03	4.5 ± 0.8	12.8 ± 0.6	236.2 ± 109.6	25.2 ± 7.6
	4	75.9 ± 2.4	0.19 ± 0.02	4.4 ± 1.3	12.30± 1.8	249.1 ± 72.6	19.6 ± 9.2
	5	74.5 ± 1.8	0.18 ± 0.04	4.1 ± 0.6	10.9 ± 3.2	216.6 ± 33.0	22.6 ± 5.2
	6	75.7 ± 1.3	0.18 ± 0.02	4.2 ± 1.5	11.3 ± 3.5	301.1 ± 142.9	23.2 ± 6.0
	7	74.7 ± 1.3	0.20 ± 0.06	5.3 ± 2.1	10.7 ± 0.9	251.1 ± 172.1	25.9 ± 12.9
ULC	**1**	73.1 ± 1.0	0.28 ± 0.07	2.9 ± 0.7	13.7 ± 1.4	172.9 ± 67.2	23.0 ± 10.9
	2	71.5 ± 4.4	0.38 ± 0.14	2.5 ± 1.1	15.2 ± 3.1	183.9 ± 74.1	21.5 ± 5.1
LLC	**1**	73.1 ± 3.2	0.22 ± 0.04	4.6 ± 0.4	13.2 ± 1.4	219.8 ± 94.8	28.2 ± 10.5
	2	71.9 ± 4.2	0.23 ± 0.06	4.0 ± 0.2	13.7 ± 2.1	163.0 ± 67.6	22.2 ± 6.6
	3	77.1 ± 13.8	0.19 ± 0.13	3.4 ± 2.0	10.7 ± 6.3	148.3 ± 54.8	18.6 ± 5.7
	4	72.9 ± 1.9	0.30 ± 0.14	5.3 ± 1.6	15.9 ± 5.7	143.7 ± 41.5	18.5 ± 7.0

Table 3
Direction-based tensile data at all testing locations: At each location, a Student's t-test was performed to compare tensile properties between the IS and AP directions. Anisotropy was observed in the tensile modulus at locations S1, S2, S3, and LLC4. Tensile modulus was greatest in the AP direction at S1, whereas it was greatest in the IS directions at the other locations.

Location		Tensile Modulus (MPa)			Ultimate Tensile Strength (MPa)		
		IS	AP	Anisotropy Index (IS/AP)	IS	AP	Anisotropy Index (IS/AP)
S	**1**	3.8 ± 1.3^{B}	7.2 ± 0.3^{A}	0.5	2.4 ± 0.8	4.3 ± 1.5	0.6
	2	12.7 ± 1.4^{A}	6.7 ± 0.4^{B}	1.9	5.2 ± 3.4	1.9 ± 0.6	2.7
	3	10.8 ± 0.5^{A}	7.6 ± 0.9^{B}	1.4	3.5 ± 1.5	4.6 ± 2.3	0.8
	4	8.0 ± 0.6	7.6 ± 0.3	1.1	3.8 ± 0.1	3.6 ± 2.1	1.1
	5	7.0 ± 3.8	3.9 ± 2.8	1.8	1.8 ± 1.1	1.6 ± 1.2	1.1
	6	4.8 ± 2.5	4.4 ± 1.9	1.1	1.7 ± 1.2	1.5 ± 0.8	1.1
	7	10.0 ± 3.7	10.1 ± 3.5	1.0	4.5 ± 3.0	2.0 ± 0.0	2.3
ULC	**1**	4.2 ± 4.1	11.5 ± 6.7	0.4	2.3 ± 0.7	4.0 ± 1.4	0.6
	2	13.3 ± 3.4	14.1 ± 4.6	0.9	4.4 ± 2.3	6.5 ± 2.2	0.7
LLC	**1**	4.4 ± 3.1	3.6 ± 3.4	1.2	2.6 ± 1.8	2.4 ± 1.9	1.1
	2	4.7 ± 1.5	3.4 ± 3.5	1.4	2.9 ± 1.0	1.9 ± 1.1	1.5
	3	6.3 ± 4.4	5.5 ± 0.4	1.1	3.4 ± 2.6	3.1 ± 1.2	1.1
	4	9.2 ± 1.4^{A}	3.2 ± 0.6^{B}	2.9	4.0 ± 2.1	2.0 ± 1.0	2.0

In the ULC and LLC, collagen appeared to be aligned in the medial-lateral (ML) direction, perpendicular to both the AP and IS directions (Supplemental Figure 1). Collagen alignment in the IS direction was not detected.

3.3. Examination of functional properties across regions of the nose

In the third level of analysis, the overall functional properties were compared among the regions of nose. To examine this, mechanical properties and biochemical content from the locations within each region were pooled. Mechanical properties were found to significantly vary by region (Fig. 3). The septum, ULC, and LLC all displayed hyperelastic behavior in tension, with strains at failure of 59.9 ± 25.3%, 77.7 ± 52.4%, and 78.2 ± 22.2%, respectively.

There were also significant differences in biochemical content among the regions (Fig. 4). DNA/DW was greater in the LLC than the septum. GAG/DW in the ULC was significantly lower than in the septum and LLC. There were no significant differences in Col/DW among the regions. There were no differences in Pyr/WW, Pyr/DW, and Pent/DW among the regions. Additionally, Pent/WW in the septum was significantly lower than in the ULC and LLC.

Significant differences in the content of collagen subtypes among the regions was also found. Collagen I (Col I)/WW, Col I/DW, and Col I/Col (Fig. 5A, Supplemental Table 2) were significantly greater in the LLC than in the septum. Collagen II (Col II)/Col (Fig. 5B) was significantly greater in the septum than in the ULC and LLC. There were no statistical differences in Col II/WW or Col II/DW among the regions (Supplemental Table 2). Additionally, collagen III (Col III)/WW, Col III/DW, and Col III/Col (Fig. 5C, Supplemental Table 2) in the LLC and ULC were significantly greater than in the septum. Fig. 5D shows the relative amounts of Col II, Col I, and other minor collagens. The ratio of Col II:Col I (i.e., degree of hyalinicity) was the greatest in the septum. Collagen VI was present in all regions, but did not vary significantly by region (Supplemental Table 2). The contents of all other minor collagens per total collagen, per WW, and per DW were minimal and not regionally different (Supplemental Table 2). Collagen I, II, and III normalized to WW and DW are also provided in Supplemental Table 2.

Histological examination showed zonal organization and regional differences through staining (Fig. 6). The septum showed a similar cellular organization to hyaline articular cartilage with bilateral symmetry. The peripheral zones (i.e., the superficial zones of cartilage that interface with the mucoperichondrium) contained flat, elongated cells oriented parallel with the edges. The central zone (i.e., the deepest zone of cartilage) showed rounded chondrocytes in lacunae organized into columns. The septum stained the most strongly for GAG compared to the ULC and LLC. Additionally, the pericellular matrix and the territorial matrix in the central zone stained strongly for GAG. Histologically, chondrons appeared to be present. The septum stained more weakly for colla-

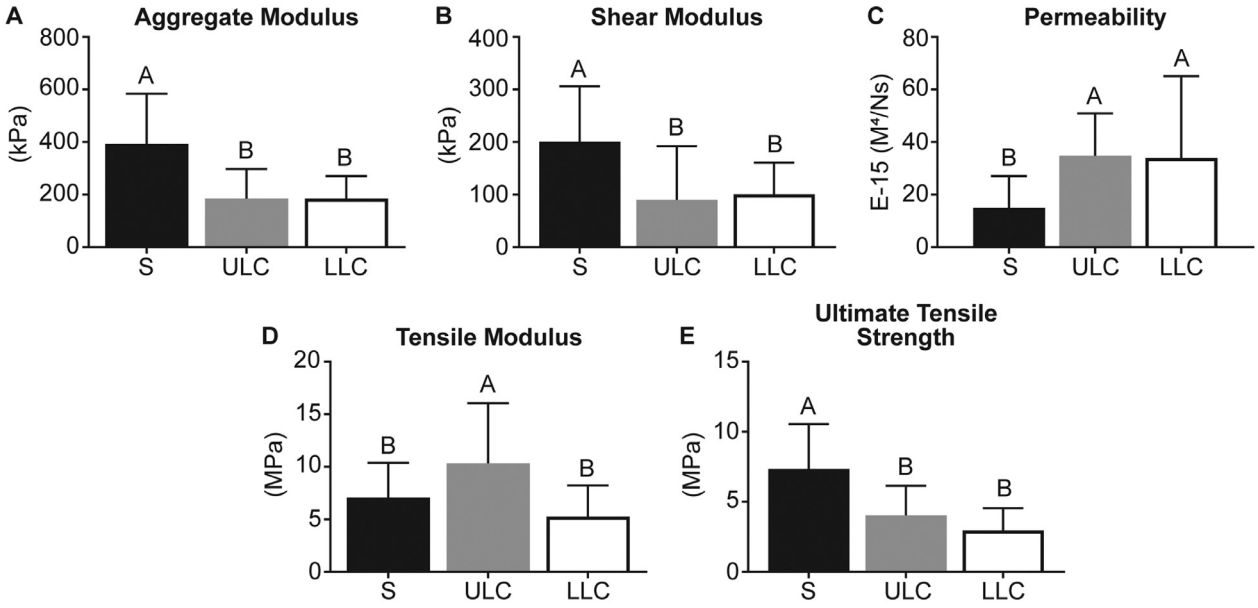

Fig. 3. Mechanical properties vary by region of the nose: A one-way ANOVA was performed among regions for all mechanical properties. A) Aggregate modulus and B) shear modulus were greatest in the septum; C) Permeability was greatest in the ULC and LLC; D) Tensile modulus was greatest in the ULC; E) UTS was greatest in the septum.

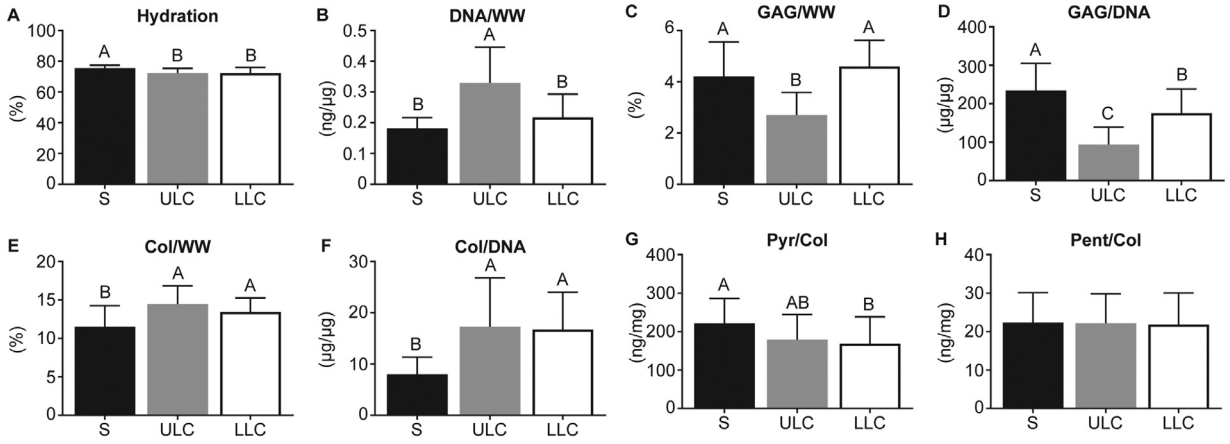

Fig. 4. Biochemical content varies by region of the nose: A one-way ANOVA was performed among regions for all biochemical contents. A) Hydration was greatest in the septum; B) DNA/WW was greatest in the ULC; C) GAG/WW was lowest in the ULC; D) GAG/DNA was greatest in the septum, followed by the LLC; E, F) Col/WW and Col/DNA were lowest in the septum; G) Pyr/Col was greater in the septum than the LLC; H) Pent/Col did not vary by region.

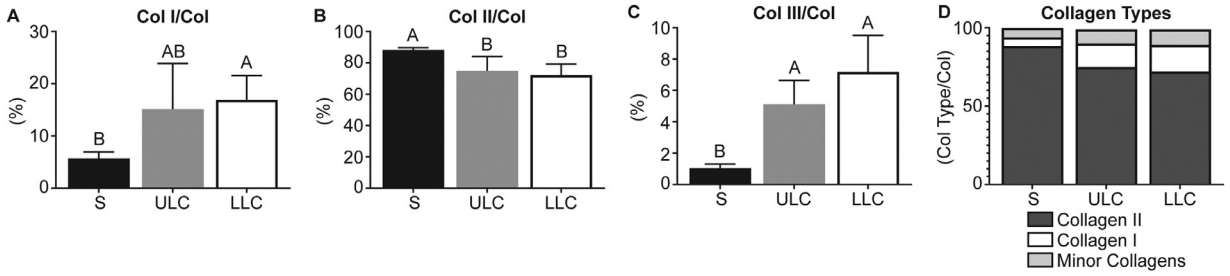

Fig. 5. Collagen types by region of the nose: For each collagen type, a one-way ANOVA was performed among regions. A) Collagen I content was greatest in the LLC and lowest in the septum; B) Collagen II content was greatest in the septum; C) Collagen III content was greatest in the ULC and LLC; D) The relative amounts of Col II, Col I, and other minor collagens indicate that the septum has a higher degree of hyalinicity than the ULC and LLC.

gen throughout the bulk of the tissue compared to the ULC and LLC. The peripheral zones of the septum showed stronger collagen staining and concentrated pericellular staining compared to the central zone.

The ULC showed less pronounced zonal cell organization, but higher cellular density. Cells were grouped into lacunae with tight pericellular staining for GAG. GAG staining was slightly more intense in the central zone than in the peripheral zones. However, this pattern was not as pronounced as in the septum. Collagen staining appeared homogeneous throughout the thickness of the ULC. Additionally, the transition between the cartilage and the surrounding mucoperichondrium tissue was less distinct than in the septum, illustrated by the dashed line in Fig. 6.

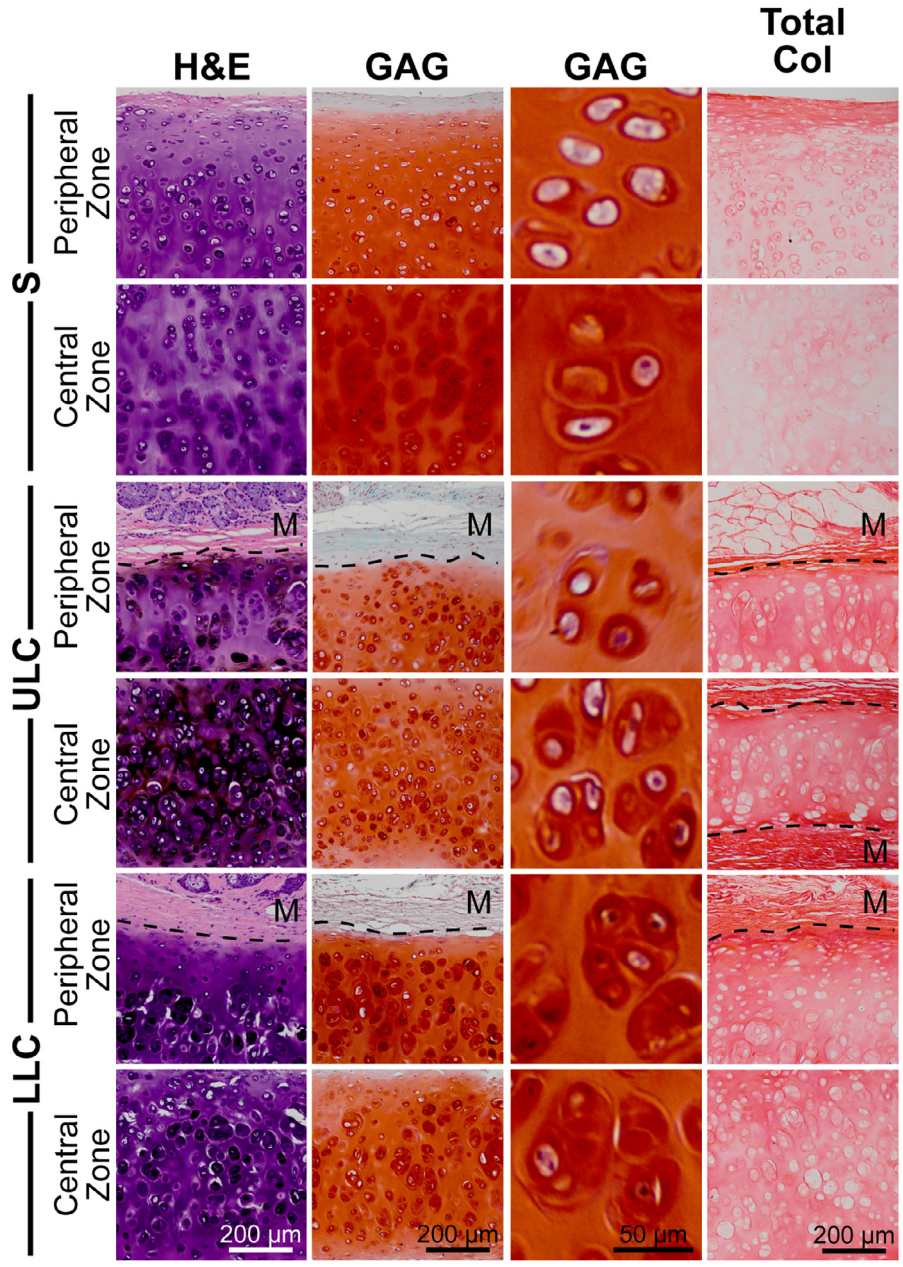

Fig. 6. Histology by regions: In all regions, peripheral zones contained flat, elongated cells oriented parallel with the edges, and central zones showed rounded chondrocytes in lacunae. The septum stained the most strongly for GAG. The ULC showed less pronounced zonal cell organization, but higher cellular density and more intense collagen staining. Strong pericellular GAG staining in all regions suggests the presence of chondrons. Black dashed lines represent the border between cartilage and mucoperichondrium, which is denoted with an "M."

The LLC had similar organization and cell morphology to the ULC. However, there was less cellular density in the central zone than in the ULC. Cells were grouped into lacunae with intense GAG staining. GAG staining was slightly more intense in the peripheral zones compared to the central zone. Collagen staining was intense and homogeneous throughout the thickness of the cartilage. The transition from cartilage to mucoperichondrium was also not as distinct in the ULC as in the septum.

3.4. Identification of structure-function relationships in nasal cartilage

Correlations between location-matched mechanical properties and biochemical content were analyzed for the septum, ULC, and LLC. Analysis of correlations of septal data were performed independently from the ULC and LLC because of the septum's higher degree of hyalinicity (Fig. 5D). Correlations were performed for the ULC and LLC by combining data from these regions. No statistically significant correlations were found in the septum. For the combined ULC and LLC, statistically significant correlations were found between the aggregate modulus and Pyr/WW, Pyr/DW, Pyr/Col, and Pent/DW, as well as between the tensile modulus and Col/WW (Fig. 7). As the amount of collagen crosslinks increased, the aggregate modulus increased linearly. Additionally, as collagen content increased, the tensile modulus increased linearly.

4. Discussion

The goals of this study were to provide a comprehensive characterization of human nasal cartilage and generate engineering de-

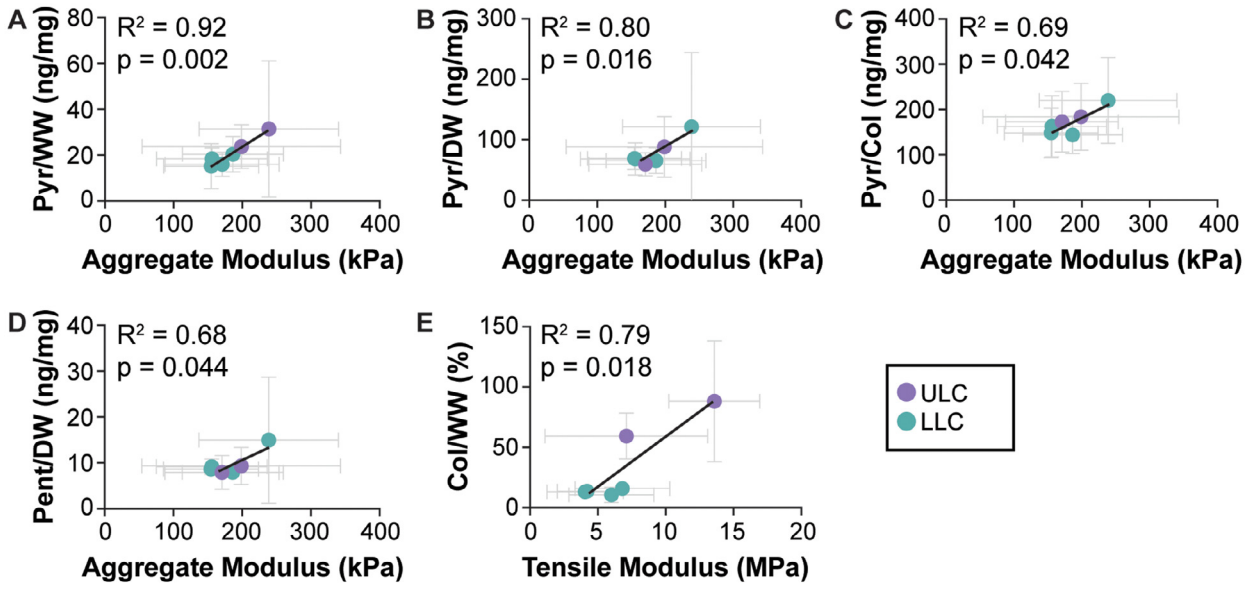

Fig. 7. Significant correlations: Data were matched by location for Pearson correlation analysis. Analysis of septal data were performed independently because of the higher degree of hyalinicity in the septum and resulted in no significant correlations. Significant correlations of location-matched data in the ULC and LLC were detected between aggregate modulus and A) Pyr/WW, B) Pyr/DW, C) Pyr/Col, and D) Pent/DW, as well as E) between tensile modulus and Col/WW.

sign criteria. The latter can be used as a benchmark of comparison for the evaluation of biomimetic cartilage tissue engineering efforts. The hypothesis that functional properties would differ based on region of nasal cartilage is supported by the data. Significant differences in mechanical properties, biochemical content, and collagen types were observed (Figs. 2-5) among regions. Cartilage from all regions exhibited hyperelasticity in tension, but regions varied in degree of hyalinicity, with the septum being the most hyaline. Qualitative differences in histological staining were also observed (Fig. 6). Within each region, no statistical differences in functional properties based on location were detected, but anisotropy at several locations within the septum and LLC was noted. To elucidate structure-function relationships, statistical correlations between mechanical properties and biochemical content were performed based on hyalinicity of anatomical region. Aggregate modulus was found to have a significant, positive correlation with pyridinoline and pentosidine content in the ULC and LLC. Additionally, tensile modulus was found to have a significant, positive correlation with total collagen content. This study represents a comprehensive dataset regarding the quantitative functional properties of human nasal cartilage, measured via methods that are standard to the field of cartilage tissue engineering.

This is the first study to measure the compressive properties of nasal cartilage using creep indentation and biphasic mixture theory, which is one of the most commonly accepted techniques for evaluating hyaline cartilages. The septum was found to have a compressive aggregate modulus over twice that of both the ULC and LLC (Fig. 3). These regional differences are supported by previous studies, which have shown the septum to have greater compressive elastic and compressive Young's moduli than the LLC [27,29]. GAG content, which has traditionally been thought to impart compressive stiffness via the attraction of water [41], was comparable in the septum and LLC. However, of the three regions, hydration was greatest, and permeability was the lowest in the septum (Fig. 4). While the negatively charged GAGs attract water, the solid extracellular matrix is responsible for resisting the efflux of water during cartilage compression [41]. The septum has been shown to contain thick sheets of collagen, which is highly organized in a broad mesh framework [42]. In contrast, the LLC was shown to have a looser, less organized arrangement of collagen [42]. Therefore, data from this study and from prior work, together, suggest that it may not be the amount of solid matrix, but rather, the organization of the matrix that results in low permeability and increased compressive aggregate modulus in the septum via the physical resistance of water leaving the tissue (Fig. 8).

In contrast to the septum, where no significant correlations were observed, aggregate modulus in the ULC and LLC was significantly correlated with the degree of collagen crosslinking. The aggregate modulus was significantly correlated with Pyr/WW, Pyr/DW, Pyr/Col, and Pent/DW (Fig. 7). Pyridinoline is a mature enzymatic collagen crosslink that is important for the tensile properties of collagenous tissues [37]. Pentosidine is an advanced glycation end-product (AGE) that results from the non-enzymatic glycation of collagen. AGEs result in stiffening of cartilage and accumulate with age [43]. Pentosidine content may play a role in tensile properties in this study because of the age of the tissue donors (60-100 years). The correlations derived from this study suggest that, in the less hyaline ULC and LLC, traditional cartilage structure-function relationships do not hold true, and that collagen crosslinking, whether by pyridinoline or pentosidine, plays a more influential role in imparting compressive stiffness.

Significant variations in the tensile properties among anatomical regions were observed. The UTS of the septum was the highest of all the regions and was 1.8 times greater than the ULC and 2.4 times greater than the LLC (Fig. 3). Additionally, the UTS of the septum observed in this study was approximately 3.8 times greater than what has previously been reported [44]. In contrast to the UTS, the ULC had the greatest tensile modulus and was 1.5 times greater than the septum and 1.9 times greater than the LLC. It was also in the range of tensile properties of human hyaline articular cartilage [41]. These regional variations in tensile modulus are supported by a previous study of nasal cartilage from three patients that showed the septum had a greater modulus of elasticity than the LLC, although statistical analysis was not performed [31]. The hyperelastic behavior of human septal cartilage that has been previously reported [44] was further supported by the high strains reached at tensile failure in this study. The high UTS of the septum is perhaps explained by the presence of higher amounts of mature collagen crosslinks compared to other regions. Pyr/Col, which is known to influence tensile properties, was greatest in the sep-

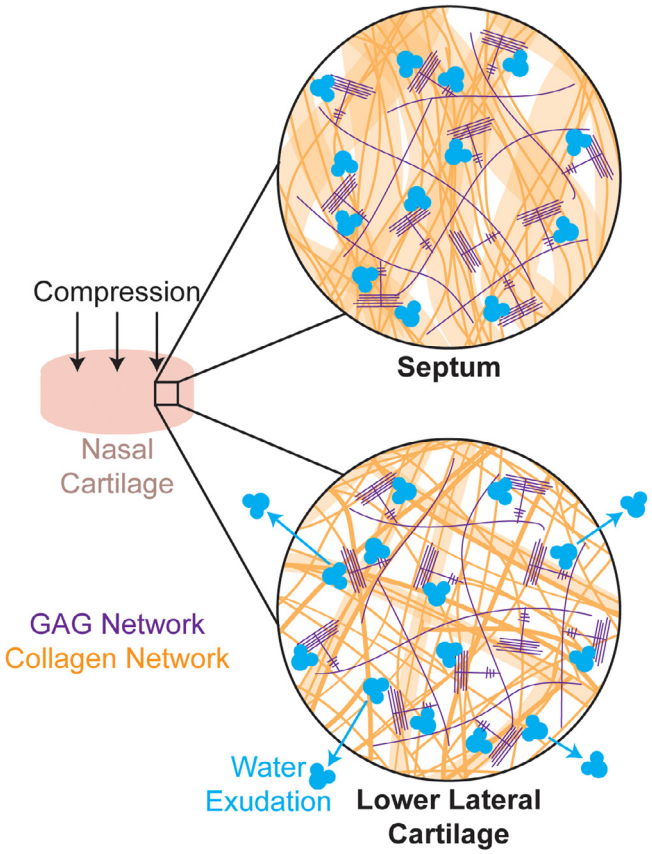

Fig. 8. Collagen organization in the septum and LLC may contribute to different tissue mechanical properties: The septum has been shown to contain thick sheets of broad, highly organized collagen fibers that may resist water exudation, resulting in lower tissue permeability and a greater compressive aggregate modulus. In contrast, the LLC has been shown to contain collagen fibers of heterogeneous thickness in a looser and less organized arrangement that may allow for more water exudation, resulting in greater tissue permeability and lower aggregate modulus.

tum (Fig. 4) [37]. Tensile modulus in the ULC and LLC was found to significantly correlate with Col/WW (Fig. 7). Thus, in nasal cartilage, it may be suggested that collagen content influences tensile stiffness, and pyridinoline crosslinking of the collagen influences tensile strength.

Tensile anisotropy was shown in the LLC, with the IS direction having a greater tensile modulus and UTS than in the AP direction (Fig. 2). When examined at each location, tensile anisotropy was observed at locations 1, 2, and 3 within the septum, as well as at location 4 in the LLC. However, when location data were pooled, tensile anisotropy was not shown in the septum or ULC. This is similar to a previous study that also found no tensile anisotropy in the septum [44]. However, it contrasts with previously reported collagen alignment of the LLC and septum [45]. The septal cartilage has been shown to have anisotropic collagen arrangement, with fibers in close proximity to the maxillary crest (base of the septum) oriented perpendicularly to the interface (vertically in the IS direction) [45]. Based on the previously reported collagen alignment, anisotropy would be expected at locations 4 and 7 in the septum. However, it was only observed at superior and anterior locations in the septum. Collagen fibers in the LLC and the central area of the septum have been shown to lack a definitive orientation [42,45]. Polarized light microscopy revealed some collagen alignment in the ML direction in the ULC and LLC, but not in the AP direction. Collagen alignment in the IS direction was not detectable. The histology sections showed the cross section of the nasal cartilage in parallel to the AP and ML planes, with the IS direction perpendicular to the visible planes. Because tensile anisotropy was detected in the IS direction, and previous studies reported IS collagen alignment, it is likely that the collagen alignment exists in the IS direction but was not visible. Additional studies should be performed to clarify collagen alignment in the context mechanical anisotropy or to elucidate another underlying source of tensile anisotropy. Furthermore, beyond achieving the appropriate tensile material properties in engineered nasal cartilage, consideration must be made to also impart the tensile anisotropy present in native nasal cartilage.

Human nasal cartilage, particularly the septum, closely resembles human articular cartilage, despite the absence of articulation in the nose. Surprisingly, the compressive aggregate modulus of the septum and the tensile modulus of the ULC were in the range of compressive stiffness and tensile stiffness, respectively, for human articular cartilage [41]. Additionally, histological staining patterns and chondrocyte morphology reflected those in articular cartilage (Fig. 6). Cell density in the septum appeared similar to the cellular density of articular cartilage [41]. In all regions, cells in the peripheral zone were elongated parallel to the edge of the tissue, akin to cell alignment near the articulating surface in articular cartilage. Cells in the central zone were rounded and arranged in columns, particularly in the septum and LLC. Furthermore, in the septum, collagen staining was most intense in the peripheral zone and GAG staining was most intense in the central zone, matching the distribution of collagen and GAG in the superficial and middle zones, respectively, in articular cartilage. The cell organization and distribution of matrix staining are supported by previous studies that show similar results [27,29,30]. Given the similarity of nasal cartilage to articular cartilage, perhaps the wealth of tissue engineering strategies for hyaline articular cartilage can be readily adapted to successfully achieve the design criteria for engineered nasal cartilage.

The presence of collagen VI suggests that chondrons may be present in all regions of nasal cartilage. A chondron consists of a chondrocyte and its pericellular matrix including collagen VI, collagen IX, perlecan, hyaluronan, and biglycan [46]. In particular, collagen VI exists almost exclusively in the pericellular matrix, with uniformly low levels present in the territorial and interterritorial matrices [47–49]. The chondron serves as a mechanical unit of cartilage to protect chondrocytes from mechanical loads that the bulk tissue experiences [47]. Chondrons are able to withstand greater forces than cells alone [50]. Histology suggested the presence of chondrons in all regions (Fig. 6). Furthermore, bottom-up proteomics also revealed the presence of collagen VI in all regions. Collagen VI is located throughout the matrix of cartilage only in the developing fetus and localizes to the pericellular matrix as cartilage matures [51,52]. While it is not possible to determine the spatial location of collagen VI via the mass spectrometry methods used in this study, it would not be expected to find collagen VI located throughout the cartilage matrix in sample donors of advanced age, such as those used in this study. Therefore, it can be suggested that the presence of collagen VI further supports the existence of chondrons in nasal cartilage. Future studies should specifically examine the presence of chondrons and other microstructural characteristics in nasal cartilage via histological staining or spatial mass spectrometry for hallmark matrix molecules, such as collagen VI and perlecan.

It is known that nasal cartilage serves a structural role to keep the external nasal airways open. Specifically, the septum resists deformation to provide midline support to the softer lateral sidewalls and to prevent nasal collapse [53]. A study using 3D computational models constructed from computed tomography (CT) scans of the nasal airways of five healthy subjects showed that average shear wall stress (i.e., a “friction force” generated when moving air contacts the nasal wall) in the septum was 0.08 Pa, with peak shear

Table 4
Additional biochemical content by region: For each biochemical content, a one-way ANOVA was performed among regions. Statistical differences among regions were observed in DNA/DW, GAG/DW, and Pent/WW.

Location	DNA/DW (ng/μg)	GAG/DW (%)	Col/DW (%)	Pyr/WW (ng/mg)	Pyr/DW (ng/mg)	Pent/WW (ng/mg)	Pent/DW (ng/mg)
S	0.73 ± 0.10^{C}	17.0 ± 15.0^{A}	46.9 ± 10.5	18.6 ± 5.9	79.3 ± 29.6	1.7 ± 0.6^{B}	7.1 ± 2.5
ULC	1.18 ± 0.33^{A}	9.8 ± 3.0^{B}	52.1 ± 5.0	20.3 ± 8.5	75.4 ± 40.3	2.3 ± 0.8^{A}	8.7 ± 3.7
LLC	0.84 ± 0.12^{B}	14.4 ± 4.4^{A}	48.7 ± 4.0	18.0 ± 7.5	67.5 ± 21.9	2.5 ± 0.6^{A}	8.6 ± 1.3

Table 5
Summary of native cartilage properties and engineering design criteria for human nasal cartilage tissue engineering. Tissue engineering (TE) criteria were based on a functionality index = 0.42, which has shown success in the repair of other cartilages *in vivo*.

	S		**ULC**		**LLC**	
	Native	**TE**	**Native**	**TE**	**Native**	**TE**
Aggregate Modulus (kPa)	393	165	185	78	185	78
Tensile Modulus (MPa)	7.1	3.0	10.3	4.3	5.3	2.2
Ultimate Tensile Strength (MPa)	7.3	3.1	4.0	1.7	3.0	1.3
GAG/WW (%)	4.2	1.8	2.7	1.1	4.6	1.9
Col/WW (%)	11.5	4.8	14.5	6.1	13.5	5.7
Pyr/Col (ng/μg)	221.5	93.0	179.2	75.3	167.0	70.1

wall stress of 0.65 Pa during resting breathing [54]. Shear stress was also shown to be concentrated in Little's area, also known as Kiesselbach's area or Kiesselbach's triangle, which is located where five main arteries in the mucoperichondrium meet, over the anterior central area of the septal cartilage [54]. Doubling the airflow rate increased the peak shear wall stress to 1 Pa but did not change the stress distribution [54]. In another study using computational fluid dynamics (CFD) based on CT scans, peak wall shear stress in healthy patients was calculated to be 1.2 Pa in the middle turbinate region, with a wall shear force of 7.47 E-4 N [55]. It has also been shown, using CFD, that increasingly large perforations in the anterior septum caused increases in shear wall stress along the septum [56]. These peak stresses are at least six orders of magnitude less than contact stresses experienced by human articular cartilage in joints (0.5 - 5.0 MPa) [57]. Despite these low calculated forces, the high mechanical capacity of nasal cartilage demonstrated in this study, particularly in the septum, suggests that nasal cartilage may experience higher mechanical loads, whether chronically or acutely, than previously realized.

The septum appeared to be more hyaline than the ULC and LLC based on the presence of collagen types. The ratio of collagen II:I was greatest in the septum, whereas, in the ULC and LLC, there was a higher relative content of collagen I and other minor collagens (Fig. 5). Interestingly, collagen III was present in all regions, with the highest content in the ULC and LLC. Collagen III is known to form covalent enzymatic collagen crosslinks, which strengthen and mature the collagen networks [37]. In fibrocartilage, collagen III forms homofibrils on its own, as well as heterofibrils with collagen I, and accounts for less than 10% of total collagen [37]. In hyaline articular cartilage, small amounts of collagen III fibers can be found superimposed on the extracellular matrix that mostly comprises collagen II [58]. Together, the presence of greater amounts of collagen I and III in the ULC and LLC compared to the septum suggest these regions to be more fibrocartilaginous. The presence of these collagens I, II, and III in varying degrees based on region suggest that nasal cartilage, while mostly hyaline, exists on a spectrum of hyalinicity Table 4.

The goal of tissue engineering is to generate biomimetic tissues for implantation. However, it has been previously shown that cartilage implants with a functionality index (FI) of 0.42 (i.e., implants that achieved 42% of native cartilage properties) resulted in complete healing of defects in the temporomandibular joint disc [59]. This suggests that a lesser degree than complete biomimicry can achieve cartilage healing. Based on the functional properties elucidated in this study and an FI = 0.42, suggested design criteria for tissue-engineered nasal cartilage are presented in Table 5. Functionality index assessment and *in vivo* studies specific to the repair of nasal cartilage should be performed to further refine the degree of biomimicry necessary for tissue-engineered nasal cartilage implants.

5. Conclusions

This study yielded a quantitative characterization of the properties of human nasal cartilage, toward the establishment of engineering design criteria for nasal cartilage tissue engineering efforts. Several aspects of nasal cartilage were shown for the first time. It was shown that nasal cartilage exhibits regional differences in functional properties and demonstrates characteristics of articular cartilage, suggesting that nasal cartilage may experience greater mechanical loading than expected. While all regions were hyaline, the septum was shown to be more hyaline than the ULC and LLC based on collagen II:I ratio. Traditional structure-function relationships in hyaline cartilage were not observed. However, the more fibrocartilaginous ULC and LLC demonstrated significant correlations between collagen crosslinks and aggregate modulus, as well as between collagen content and tensile modulus. Histology and collagen VI content suggested the presence of chondrons in all regions. Future studies should further investigate the mechanical capacity and function of nasal cartilage and the presence of chondrons within the tissue, as well as validate the structure-function relationships identified in this study by further developing mathematical models or mechanisms of interaction. This study represents a substantial stride forward in the understanding of human nasal cartilage properties. In addition to establishing engineering design criteria, these data provide context for further exploration or clarification of characteristics, such as tensile anisotropy, collagen alignment, and gender- or age-based differences in properties.

Declaration of Competing Interests

The authors declare that they have no known competing financial interests or personal relationships that could have appeared to influence the work reported in this paper

Acknowledgements

The authors wish to thank individuals who donate their bodies and tissues for the advancement of education and research.

Funding

This work was supported by the Henry Samueli Endowed Chair for Kyriacos A. Athanasiou and the L'Oréal USA For Women in Science fellowship program, in partnership with the American Association for the Advancement of Science (AAAS).

Supplementary materials

Supplementary material associated with this article can be found, in the online version, at doi:10.1016/j.actbio.2023.07.011.

References

[1] S.H.J. Andrews, M. Kunze, A. Mulet-Sierra, L. Williams, K. Ansari, M. Osswald, A.B. Adesida, Strategies to mitigate variability in engineering human nasal cartilage, Sci. Rep. 7 (2017).
[2] S.H.J. Andrews, M. Kunze, A. Mulet-Sierra, L. Williams, K. Ansari, M. Osswald, A.B. Adesida, Author correction: strategies to mitigate variability in engineering human nasal cartilage, Sci. Rep. 9 (1) (2019) 17115.
[3] J.L. Arnholt, Thermal injuries, otolaryngology/head and neck combat casualty care.
[4] P.J. Belmont Jr., B.J. McCriskin, R.N. Sieg, R. Burks, A.J. Schoenfeld, Combat wounds in Iraq and Afghanistan from 2005 to 2009, J. Trauma Acute Care Surg. 73 (1) (2012) 3–12.
[5] D.G. Roblin, R. Eccles, What, if any, is the value of septal surgery? Clin. Otolaryngol. 27 (2) (2002) 77–80.
[6] A.S. Bruce, M.S. Aloia, S. Ancoli-Israel, Neuropsychological effects of hypoxia in medical disorders, in: Assessment of Neuropsychiatric and Neuromedical Disorders, Oxford University Press, New York, NY, 2009, pp. 336–349.
[7] M. Rankin, G.L. Borah, Perceived functional impact of abnormal facial appearance, Plast. Reconstr. Surg. 111 (7) (2003) 2140–2146.
[8] C. Kucur, O. Kuduban, A. Ozturk, M.S. Gozeler, I. Ozbay, E. Deveci, E. Simsek, Z. Kaya, Psychological evaluation of patients seeking rhinoplasty, Eurasian J. Med. 48 (2) (2016) 102–106.
[9] E. Spataro, G.H. Branham, Principles of Nasal Reconstruction, Facial Plast. Surg. 33 (1) (2017) 9–16.
[10] W. Pirsig, E.B. Kern, T. Verse, Reconstruction of anterior nasal septum: back–to-back autogenous ear cartilage graft, Laryngoscope 114 (4) (2004) 627–638.
[11] J.H. Wee, M.H. Park, S. Oh, H.R. Jin, Complications associated with autologous rib cartilage use in rhinoplasty: a meta-analysis, JAMA Facial Plast. Surg. 17 (1) (2015) 49–55.
[12] D.J. Menger, G.J. Nolst Trenite, Irradiated homologous rib grafts in nasal reconstruction, Arch. Facial Plast. Surg. 12 (2) (2010) 114–118.
[13] J.H. Wee, S.J. Mun, W.S. Na, H. Kim, J.H. Park, D.K. Kim, H.R. Jin, Autologous vs irradiated homologous costal cartilage as graft material in rhinoplasty, JAMA Facial Plast. Surg. 19 (3) (2017) 183–188.
[14] K. Patel, K. Brandstetter, Solid implants in facial plastic surgery: potential complications and how to prevent them, Facial Plast. Surg. 32 (5) (2016) 520–531.
[15] K. Stelter, S. Strieth, A. Berghaus, Porous polyethylene implants in revision rhinoplasty: chances and risks, Rhinology 45 (4) (2007) 325–331.
[16] A.A. Winkler, Z.M. Soler, P.L. Leong, A. Murphy, T.D. Wang, T.A. Cook, Complications associated with alloplastic implants in rhinoplasty, Arch. Facial Plast. Surg. 14 (6) (2012) 437–441.
[17] Y.K. Kim, S. Shin, N.H. Kang, J.H. Kim, Contracted nose after silicone implantation: a new classification system and treatment algorithm, Arch. Plast. Surg. 44 (1) (2017) 59–64.
[18] American Society of Plastic Surgeons, Plastic Surgery Statistics Report, 2016.
[19] K.C. Neaman, A.K. Boettcher, V.H. Do, C. Mulder, M. Baca, J.D. Renucci, D.L. VanderWoude, Cosmetic rhinoplasty: revision rates revisited, Aesthet. Surg. J. 33 (1) (2013) 31–37.
[20] N. Bateman, N.S. Jones, Retrospective review of augmentation rhinoplasties using autologous cartilage grafts, J. Laryngol. Otol. 114 (7) (2000) 514–518.
[21] M.K. Neuman, K.K. Briggs, K. Masuda, R.L. Sah, D. Watson, A compositional analysis of cadaveric human nasal septal cartilage, Laryngoscope 123 (9) (2013) 2120–2124.
[22] M.R. Homicz, K.B. McGowan, L.M. Lottman, G. Beh, R.L. Sah, D. Watson, A compositional analysis of human nasal septal cartilage, Arch. Facial Plast. Surg. 5 (1) (2003) 53–58.
[23] N. Rotter, G. Tobias, M. Lebl, A.K. Roy, M.C. Hansen, C.A. Vacanti, L.J. Bonassar, Age-related changes in the composition and mechanical properties of human nasal cartilage, Arch. Biochem. Biophys. 403 (1) (2002) 132–140.
[24] N. Paul, K. Messinger, Y.F. Liu, D.I. Kwon, C.H. Kim, J.C. Inman, A model to estimate L-strut strength with an emphasis on thickness, JAMA Facial Plast. Surg. 18 (4) (2016) 269–276.
[25] Y.F. Liu, K. Messinger, J.C. Inman, Yield Strength Testing in Human Cadaver Nasal Septal Cartilage and L-Strut Constructs, JAMA Facial Plast. Surg. 19 (1) (2017) 40–45.
[26] M.J. Glasgold, Y.P. Kato, D. Christiansen, J.A. Hauge, A.I. Glasgold, F.H. Silver, Mechanical properties of septal cartilage homografts, Otolaryngol. Head Neck Surg. 99 (4) (1988) 374–379.
[27] M.F. Griffin, Y. Premakumar, A.M. Seifalian, M. Szarko, P.E. Butler, Biomechanical characterisation of the human nasal cartilages; implications for tissue engineering, J. Mater. Sci. Mater. Med. 27 (1) (2016) 11.
[28] J.D. Richmon, A. Sage, W.V. Wong, A.C. Chen, R.L. Sah, D. Watson, Compressive biomechanical properties of human nasal septal cartilage, Am. J. Rhinol. 20 (5) (2006) 496–501.
[29] E.J. Bos, M. Pluemeekers, M. Helder, N. Kuzmin, K. van der Laan, M.L. Groot, G. van Osch, P. van Zuijlen, Structural and Mechanical Comparison of Human Ear, Alar, and Septal Cartilage, Plast. Reconstr. Surg. Glob. Open 6 (1) (2018) e1610.
[30] M. Popko, R.L. Bleys, J.W. De Groot, E.H. Huizing, Histological structure of the nasal cartilages and their perichondrial envelope. I. The septal and lobular cartilage, Rhinology 45 (2) (2007) 148–152.
[31] R.W. Westreich, H.W. Courtland, P. Nasser, K. Jepsen, W. Lawson, Defining nasal cartilage elasticity: biomechanical testing of the tripod theory based on a cantilevered model, Arch. Facial Plast. Surg. 9 (4) (2007) 264–270.
[32] K.A. Athanasiou, A. Agarwal, A. Muffoletto, F.J. Dzida, G. Constantinides, M. Clem, Biomechanical properties of hip cartilage in experimental animal models, Clin. Orthop. Relat. Res. 316 (1995) 254–266.
[33] V.C. Mow, M.C. Gibbs, W.M. Lai, W.B. Zhu, K.A. Athanasiou, Biphasic indentation of articular cartilage–II. A numerical algorithm and an experimental study, J. Biomech. 22 (8-9) (1989) 853–861.
[34] D.D. Cissell, J.M. Link, J.C. Hu, K.A. Athanasiou, A Modified Hydroxyproline Assay Based on Hydrochloric Acid in Ehrlich's Solution Accurately Measures Tissue Collagen Content, Tissue engineering. Part C, Methods 23 (4) (2017) 243–250.
[35] B.J. Bielajew, J.C. Hu, K.A. Athanasiou, Methodology to Quantify Collagen Subtypes and Crosslinks: Application in Minipig Cartilages, Cartilage 13 (2_Suppl) (2021) 1742s–1754s.
[36] C. Greiner, S. Grainger, S. Farrow, A. Davis, J.L. Su, M.D. Saybolt, R. Wilensky, S. Madden, S.T. Sum, Robust quantitative assessment of collagen fibers with picrosirius red stain and linearly polarized light as demonstrated on atherosclerotic plaque samples, PloS one 16 (3) (2021) e0248068.
[37] B.J. Bielajew, J.C. Hu, K.A. Athanasiou, Collagen: quantification, biomechanics, and role of minor subtypes in cartilage, Nat. Rev. Mater. 5 (10) (2020) 730–747.
[38] W.E. Brown, G.D. DuRaine, J.C. Hu, K.A. Athanasiou, Structure-function relationships of fetal ovine articular cartilage, Acta biomaterialia 87 (2019) 235–244.
[39] E.Y. Salinas, G.A. Otarola, H. Kwon, D. Wang, J.C. Hu, K.A. Athanasiou, Topographical Characterization of the Young, Healthy Human Femoral Medial Condyle, Cartilage (2022) 19476035221141421.
[40] JMP, JMP Statistics and Graphics Guide, Release 7 126.
[41] K.A. Athanasiou, E.M. Darling, G.D. DuRaine, J.C. Hu, A.H. Reddi, Articular Cartilage, CRC Press, Boca Raton, FL, 2017 Second ed..
[42] P.K. Holden, L.H. Liaw, B.J. Wong, Human nasal cartilage ultrastructure: characteristics and comparison using scanning electron microscopy, Laryngoscope 118 (7) (2008) 1153–1156.
[43] D.M. Saudek, J. Kay, Advanced glycation endproducts and osteoarthritis, Curr. Rheumatol. Rep. 5 (1) (2003) 33–40.
[44] J.D. Richmon, A.B. Sage, V.W. Wong, A.C. Chen, C. Pan, R.L. Sah, D. Watson, Tensile biomechanical properties of human nasal septal cartilage, Am. J. Rhinol. 19 (6) (2005) 617–622.
[45] F. Aksoy, Y.S. Yildirim, H. Demirhan, O. Ozturan, S. Solakoglu, Structural characteristics of septal cartilage and mucoperichondrium, J. Laryngol. Otol. 126 (1) (2012) 38–42.
[46] R.E. Wilusz, J. Sanchez-Adams, F. Guilak, The structure and function of the pericellular matrix of articular cartilage, Matrix Biol. 39 (2014) 25–32.
[47] C.A. Poole, Articular cartilage chondrons: form, function and failure, J. Anat. 191 (1997) 1–13 (Pt 1)(Pt 1).
[48] C.A. Poole, S. Ayad, J.R. Schofield, Chondrons from articular cartilage: I. Immunolocalization of type VI collagen in the pericellular capsule of isolated canine tibial chondrons, J. Cell Sci. 90 (1988) 635–643 (Pt 4).
[49] C.A. Poole, S. Ayad, R.T. Gilbert, Chondrons from articular cartilage. V. Immunohistochemical evaluation of type VI collagen organisation in isolated chondrons by light, confocal and electron microscopy, J. Cell Sci. 103 (Pt 4) (1992) 1101–1110.
[50] J. Zhang, L. Liu, Z. Gao, L. Li, X. Feng, W. Wu, Q. Ma, X. Cheng, F. Chen, T. Mao, Novel approach to engineer implantable nasal alar cartilage employing marrow precursor cell sheet and biodegradable scaffold, J. Oral Maxillofac. Surg. 67 (2) (2009) 257–264.
[51] E.H. Morrison, M.W. Ferguson, M.T. Bayliss, C.W. Archer, The development of articular cartilage: I. The spatial and temporal patterns of collagen types, J. Anat. 189 (Pt 1) (1996) 9–22.
[52] D.R. Eyre, The collagens of articular cartilage, Semin Arthritis Rheum. 21 (3 Suppl 2) (1991) 2–11.
[53] L. Lavernia, W.E. Brown, B.J.F. Wong, J.C. Hu, K.A. Athanasiou, Toward tissue-engineering of nasal cartilages, Acta biomaterialia 88 (2019) 42–56.
[54] N. Bailie, B. Hanna, J. Watterson, G. Gallagher, A model of airflow in the nasal cavities: implications for nasal air conditioning and epistaxis, Am. J. Rhinol. Allergy 23 (3) (2009) 244–249.

[55] C. Li, A.A. Farag, G. Maza, S. McGhee, M.A. Ciccone, B. Deshpande, E.A. Pribitkin, B.A. Otto, K. Zhao, Investigation of the abnormal nasal aerodynamics and trigeminal functions among empty nose syndrome patients, Int. Forum Allergy Rhinol. 8 (3) (2018) 444–452.
[56] D.E. Cannon, D.O. Frank, J.S. Kimbell, D.M. Poetker, J.S. Rhee, Modeling nasal physiology changes due to septal perforations, Otolaryngol. Head Neck Surg. 148 (3) (2013) 513–518.
[57] R.A. Brand, Joint contact stress: a reasonable surrogate for biological processes? Iowa Orthop. J. 25 (2005) 82–94.
[58] J.J. Wu, M.A. Weis, L.S. Kim, D.R. Eyre, Type III collagen, a fibril network modifier in articular cartilage, J. Biol. Chem. 285 (24) (2010) 18537–18544.
[59] N. Vapniarsky, L.W. Huwe, B. Arzi, M.K. Houghton, M.E. Wong, J.W. Wilson, D.C. Hatcher, J.C. Hu, K.A. Athanasiou, Tissue engineering toward temporomandibular joint disc regeneration, Sci. Transl. Med. 10 (446) (2018).